

Constraining holographic cosmology using Planck data

Niayesh Afshordi,^{1,2} Elizabeth Gould,^{1,2} and Kostas Skenderis³

¹*Perimeter Institute for Theoretical Physics,
31 Caroline St. N., Waterloo, ON, N2L 2Y5, Canada*

²*Department of Physics and Astronomy,
University of Waterloo, Waterloo, ON, N2L 3G1, Canada*

³*STAG Research Centre and Mathematical Sciences, Highfield,
University of Southampton, SO17 1BJ Southampton, UK*

(Dated: June 2, 2017)

Abstract

Holographic cosmology offers a novel framework for describing the very early Universe in which cosmological predictions are expressed in terms of the observables of a three dimensional quantum field theory (QFT). This framework includes conventional slow-roll inflation, which is described in terms of a strongly coupled QFT, but it also allows for qualitatively new models for the very early Universe, where the dual QFT may be weakly coupled. The new models describe a universe which is non-geometric at early times. While standard slow-roll inflation leads to a (near-)power-law primordial power spectrum, perturbative superrenormalizable QFT's yield a new holographic spectral shape. Here, we compare the two predictions against cosmological observations. We use CosmoMC to determine the best fit parameters, and MultiNest for Bayesian Evidence, comparing the likelihoods. We find that the dual QFT should be non-perturbative at the very low multipoles ($l \lesssim 30$), while for higher multipoles ($l \gtrsim 30$) the new holographic model, based on perturbative QFT, fits the data just as well as the standard power-law spectrum assumed in Λ CDM cosmology. This finding opens the door to applications of non-perturbative QFT techniques, such as lattice simulations, to observational cosmology on gigaparsec scales and beyond.

I. INTRODUCTION

The current observational data in cosmology are fit very well by the six-parameter Λ CDM model. This model is an empirical parametrization for cosmology, combining four parameters of the transfer function with two of the primordial power spectrum. For the transfer function, the parameters correspond to the matter contents of the universe, the current rate of expansion of the universe, and the optical depth (which is related to the time of reionization). This part is well-understood in the context of the Λ CDM framework. The other two parameters, Δ_0^2 and n_s , are those of the scalar primordial power spectrum $\mathcal{P}(q)$, which is taken to have a power-law form:

$$\mathcal{P}(q) = \Delta_0^2 \left(\frac{q}{q_*} \right)^{n_s-1}, \quad (1)$$

where q_* , the pivot scale, is an (arbitrary) reference scale.

Typically the primordial power spectrum is explained using slow-roll inflation in which the early universe undergoes a phase of rapid accelerated expansion. This is used to explain the homogeneity and isotropy of the universe by having the expansion increase the size of the regions which were in causal contact after the big bang to our entire visible universe as well as making it look flat by being large enough that the curvature is not visible. In addition, starting from the quantum adiabatic vacuum, inflationary models typically predict a primordial power spectrum well approximated by the power-law form (1). While inflation is often considered to be the best scenario to explain cosmological observations, it suffers from shortcomings such as predictivity and falsifiability, sparking a search for alternative possibilities (e.g., [1]).

One of the main issues one is faced with when calculating the predictions of models for the early universe is that quantum gravity effects become relevant, while we do not yet have a full theory of quantum gravity. Inflation bypasses this by requiring that the gravitational coupling is weak enough so that only a quantum field theory on curved space-time is required. This may be sufficient for explaining (1) but it still leaves open the question of what happens at earlier times – inflation does not resolve the issue of the initial singularity. Moreover, the theory is still generically sensitive to UV issues, as radiative corrections can significantly alter the inflationary action. For these reasons, it is important to embed inflation into a UV complete theory.

Insight from the study of black hole entropy has long indicated that gravity might have a holographic nature [2, 3], *i.e.* that there is a dual quantum field theory (QFT) in one lower dimension without gravity. This principle, the holographic principle, should also apply to the early universe. Explicit examples of holographic dualities were found in string theory [4]. However, these cases tend to apply to theories with a negative cosmological constant, which is in contrast to cosmological observations.

The extension of the duality to de Sitter spacetime and cosmology was considered soon after the initial work on Anti-de Sitter space [5–9]. In the cosmological context, the statement of the duality is that the partition function of the dual QFT computes the wavefunction of the universe [9], using which, cosmological observables may be obtained. These dualities are less understood than the standard AdS/CFT duality, in part because we currently have no explicit realization in string theory. Nevertheless, one may set-up a holographic dictionary [10–14] using a correspondence [15] between cosmological accelerating solutions and holographic renormalization group (RG) flows, solutions that admit standard holographic

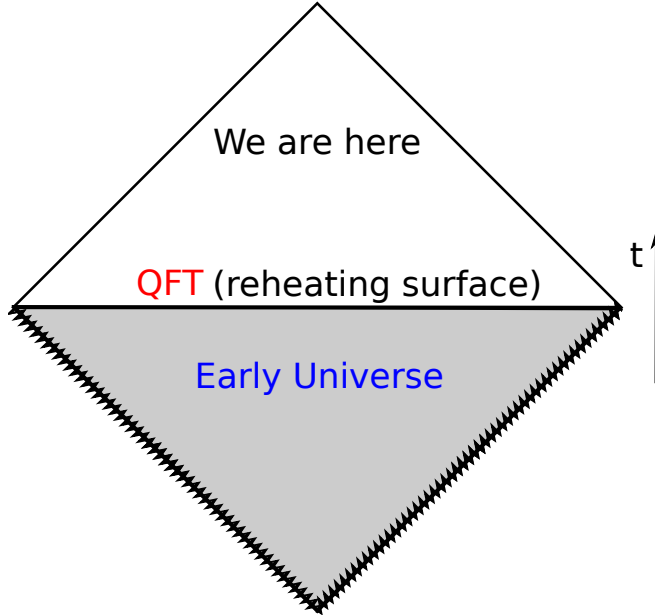


FIG. 1. A sketch of the Penrose diagram describing holographic cosmology (HC). The early Universe is non-geometric and is described by a dual QFT, which is located at the end of the non-geometric phase.

interpretation.

In this duality, time evolution is mapped to inverse renormalization group flow and the physics of the early universe is mapped to the IR physics of the dual QFT. Thus, depending on the nature of the IR, we have different cosmological scenarios. In this paper, we test theories for the very early Universe against the cosmic microwave background (CMB) data, so more precisely we would like to know what the dual QFT is which is relevant at the energy scales probed by the CMB.

One of the main properties of the holographic dualities is that they are strong/weak coupling dualities. This means that when one of the two sides is strongly coupled, and therefore difficult if not impossible to solve, the other side is weakly coupled, and solvable perturbatively. Therefore a weakly coupled inflationary period is dual to a strongly coupled quantum field theory. While work has been done in using holography in this setting (see [16–33] for a sample of works in this direction) we here mainly examine the opposite case. This is the case of a strongly coupled gravitational theory. In this case, the early universe does not have a well defined geometry. It can not be examined without quantum gravity. However, the dual QFT not only can be examined, but is weakly coupled and solvable perturbatively. This is the alternative model we examine, which we call the holographic model or holographic cosmology here.¹ In this case the dual QFT is a super-renormalizable three-dimensional QFT.² This model for the very early Universe was first proposed in [10] and it was subsequently analyzed in [11–14, 37, 38]. A sketch of the Penrose diagram describing holographic cosmology is shown in Figure 1.

Previously, this holographic model had been compared to WMAP7. It was found to be

¹ As inflation is also holographic, this is a potentially confusing terminology. Here we want to distinguish between a cosmology which has a conventional spacetime description (inflation) and one without such description (holographic cosmology).

² An example of such QFT is the worldvolume theory of coincident D2-branes. The holography nature of this theory is well established [34–36].

viable [39, 40] but mildly disfavoured relative to Λ CDM. With the release of the Planck data, it is time to reexamine the viability of the holographic model for early universe cosmology. Our results were announced in [41] and the purpose of this paper is to provide a more detailed and comprehensive discussion of their derivation.

The structure of the paper is as follows. In Section II, we describe the two models we are comparing. In Section III, we find and explain the best fit model. Section IV explains how well the two models fit the data and compare to each other. Finally, in Section V we present some concluding remarks.

II. MODELS

A. Holography for cosmology: basics

The idea of holography for cosmology is that the dual QFT computes the wavefunction of the Universe [9]. Schematically, this works as follows: The wavefunction is equal to the partition function of the dual QFT,

$$\psi(\Phi) = Z_{QFT}[\Phi], \quad (2)$$

where Φ on the left-hand side denotes collectively gravitational perturbations and on the right-hand side sources that couple to gauge invariant operators. Note that we consider the wavefunction of perturbations only in this paper. Cosmological observables may be computed using standard quantum mechanics

$$\langle \Phi(x_1) \cdots \Phi(x_n) \rangle = \int D\Phi |\psi|^2 \Phi(x_1) \cdots \Phi(x_n), \quad (3)$$

where the correlators are evaluated at end of the early universe phase (for example, at the end of the inflationary phase, if inflation describes the very early universe). Using that $Z_{QFT}[\Phi]$ may be expressed in terms of correlation functions

$$Z_{QFT}[\Phi] = \exp \left(\sum_n \frac{(-1)^n}{n!} \langle O(x_1) \cdots O(x_n) \rangle \Phi(x_1) \cdots \Phi(x_n) \right), \quad (4)$$

where O denotes the gauge invariant operators to which Φ couples.³ We now may express cosmological observables in terms of QFT correlation functions. If the QFT is strongly coupled, then the bulk is described by Einstein gravity and these results should match those coming from standard inflationary cosmological perturbation theory, while if the QFT is weakly coupled the bulk is non-geometric.

There is currently no first principles derivation of the QFT relevant for cosmology but one may use the domain-wall/cosmology correspondence [15] to map the cosmology problem to that of standard gauge/gravity duality, then use the QFT dual to the domain-wall and finally map the results back to cosmology [10, 11].⁴ This leads to the following holographic formulae for the scalar and tensor spectra, \mathcal{P} and \mathcal{P}_T , respectively,

$$\mathcal{P}(q) = -\frac{q^3}{16\pi^2} \frac{1}{\text{Im}B(q)}, \quad \mathcal{P}_T(q) = -\frac{2q^3}{\pi^2} \frac{1}{\text{Im}A(q)}, \quad (5)$$

³ We take the QFT to be Euclidean, though this is not essential.

⁴ There is a proposed duality [42] where the QFT is defined a priori (i.e. without the need to map the problem to the domain-wall first) but in this case the bulk involves Vasiliev's higher spin gravity instead of Einstein gravity.

where A, B are extracted from the momentum space 2-point function of the energy momentum tensor T_{ij} ,

$$\langle\langle T_{ij}(q)T_{kl}(-q)\rangle\rangle = A(q)\Pi_{ijkl} + B(q)\pi_{ij}\pi_{kl}. \quad (6)$$

Here $\langle T_{ij}(q_1)T_{kl}(q_2)\rangle = (2\pi)^3\delta^3(q_1 + q_2)\langle\langle T_{ij}(q_1)T_{kl}(-q_1)\rangle\rangle$, $\pi_{ij} = \delta_{ij} - q_iq_j/q^2$ is a transverse projector and $\Pi_{ijkl} = 1/2(\pi_{ik}\pi_{jl} + \pi_{il}\pi_{jk} - \pi_{ij}\pi_{kl})$ is a transverse-traceless projector. In other words, the scalar power spectrum is associated with the 2-point function of the trace of the energy-momentum tensor while the tensor power spectrum is related with the transverse-traceless part of the 2-point function. These formulae were derived for QFTs that admit a 't Hooft large N limit and they either become conformal in the UV or approach a QFT with a generalized conformal structure (where generalized conformal structure is explained in the next subsection). The imaginary part in (5) is taken after the analytic continuation,

$$q \rightarrow -iq, \quad N \rightarrow -iN, \quad (7)$$

where q is the magnitude of the momentum vector and we assume that we are dealing with an $SU(N)$ gauge theory coupled to matter in the adjoint representation, as is the case below.⁵ Similarly, one can relate the bispectra with 3-point functions of the energy momentum tensor [12–14].

When the QFT is strongly coupled, the bulk is geometric and there is a conventional description in terms of quasi-de Sitter or power law inflation. In these cases, (5) correctly reproduces the results of cosmological perturbation theory [10, 11]. Here we focus on the opposite regime where the QFT is weakly coupled.

B. Non-geometric models

In non-geometric models, the theory is defined by giving the dual QFT. Here we analyze the model proposed in [10, 11], in which the QFT is an $SU(N)$ gauge theory coupled to scalars Φ^M and fermions ψ^L , where M, L are flavor indices. The action is given by

$$S = \frac{1}{g_{\text{YM}}^2} \int d^3x \text{tr} \left[\frac{1}{2} F_{ij} F^{ij} + \delta_{M_1 M_2} \mathcal{D}_i \Phi^{M_1} \mathcal{D}^i \Phi^{M_2} + 2\delta_{L_1 L_2} \bar{\psi}^{L_1} \gamma^i \mathcal{D}_i \psi^{L_2} + \sqrt{2}\mu_{ML_1 L_2} \Phi^M \bar{\psi}^{L_1} \psi^{L_2} + \frac{1}{6} \lambda_{M_1 M_2 M_3 M_4} \Phi^{M_1} \Phi^{M_2} \Phi^{M_3} \Phi^{M_4} \right], \quad (8)$$

where all fields, $\varphi = \varphi^a T^a$, are in the adjoint of $SU(N)$ and $\text{tr} T^a T^b = \frac{1}{2} \delta^{ab}$. F_{ij} is the Yang-Mills field strength, and \mathcal{D} is a gauge covariant derivative. The Yukawa couplings μ and the quartic-scalar couplings λ are dimensionless, while g_{YM}^2 has dimension 1.

This theory is superrenormalizable and has the important property that has a “generalized conformal structure.” This means that if one promotes g_{YM}^2 to a new field that transforms appropriately under conformal transformation, the theory becomes conformally invariant [36, 43]. Related to this: if one assigns “4d dimensions” to the fields, $[A] = [\Phi^M] = 1, [\Phi^L] = 3/2$, then all terms in the action scale the same way. While this is not a symmetry of the theory, it still has implications.

⁵ In the case of a large N vector model, we need $N \rightarrow -N$.

In our case, the generalized conformal structure and the large N limit implies that the 2-point function takes the form

$$A(q, N) = q^3 N^2 f_T(g_{\text{eff}}^2), \quad B(q, N) = \frac{1}{4} q^3 N^2 f(g_{\text{eff}}^2) \quad (9)$$

where $f_T(g_{\text{eff}}^2)$ and $f(g_{\text{eff}}^2)$ are (at this stage) general functions of their argument and $g_{\text{eff}}^2 = g_{YM}^2 N/q$ is the effective dimensionless 't Hooft coupling constant. The factor q^3 reflects the fact that the energy momentum tensor has dimension 3 in three dimensions and the factor of N^2 is due to the fact that we are considering the leading term in the large N limit. The factor of $1/4$ in B is conventional.

Under the analytic continuation (7)

$$q^3 N^2 \rightarrow -iq^3 N^2, \quad g_{\text{eff}}^2 \rightarrow g_{\text{eff}}^2, \quad (10)$$

so for this class of theories one may readily perform the analytic continuation and (5) becomes

$$\mathcal{P}(q) = \frac{q^3}{4\pi^2 N^2 f(g_{\text{eff}}^2)}, \quad \mathcal{P}_T(q) = \frac{2q^3}{\pi^2 N^2 f_T(g_{\text{eff}}^2)}. \quad (11)$$

We have thus now arrived in a relation between cosmological observables and correlators of standard QFT.

Perturbation theory applies when $g_{\text{eff}}^2 \ll 1$. Since $g_{\text{eff}}^2 = g_{YM}^2 N/q$, $g_{\text{eff}}^2 \rightarrow 0$, as $q \rightarrow \infty$, reflecting the fact that the theory is super-renormalizable. On the other hand the effective coupling grows in the IR, so the question of whether the theory is perturbative or not depends on the scales we probe. In the perturbative regime, the functions f and f_T up to 2-loops take the form

$$f(g_{\text{eff}}^2) = f_0 \left(1 - f_1 g_{\text{eff}}^2 \ln g_{\text{eff}}^2 + f_2 g_{\text{eff}}^2 + O(g_{\text{eff}}^4) \right), \quad (12)$$

$$f_T(g_{\text{eff}}^2) = f_{T0} \left(1 - f_{T1} g_{\text{eff}}^2 \ln g_{\text{eff}}^2 + f_{T2} g_{\text{eff}}^2 + O(g_{\text{eff}}^4) \right). \quad (13)$$

The coefficients f_0 and f_{T0} come from 1-loop and have been computed in [10, 11]. The 2-loop computation is discussed in detail in [44]. At 2-loops there are both UV and IR divergences and these induce the log terms. Both A and B suffer from UV divergences and these can be removed with a counterterm. If (some of) the scalars in (8) are non-minimally coupled scalars⁶ then the B form factor (but not the A) also has an IR divergence. It is believed that this class of theories is non-perturbatively IR finite, with the Yang-Mills coupling effectively playing the role of an IR cut-off [45, 46]. In summary, f_1 and f_{1T} can be computed unambiguously in perturbation theory, while f_2, f_{2T} are scheme dependent and f_2 also has an IR ambiguity. As discussed in [41], we fix the scheme dependence by setting the RG scale μ equal to the pivot scale q_* , $\mu = q_*$, and the IR ambiguity of f_2 by setting the IR cut-off equal to g_{YM} .

Following [40], we define new dimensionless variables g, β, g_T, β_T via ⁷

$$f_1 g_{YM}^2 N = g q_*, \quad \ln \beta = -\frac{f_2}{f_1} - \ln |f_1|, \quad f_{1T} g_{YM}^2 N = g_t q_*, \quad \ln \beta_t = -\frac{f_{T2}}{f_{T1}} - \ln |f_{T1}| \quad (14)$$

⁶ When non-minimal scalars are coupled to gravity, their action contains a coupling to curvature, $\int \xi R \Phi^2$. Correspondingly, their energy-momentum tensor contains a new term proportional to the so-called improvement term.

⁷ This parametrization assumes that $f_1 \neq 0, f_{1T} \neq 0$. While generically this is true, there are also examples where this does not hold. For example, (8) with only scalars has $f_1 = 0$. These cases require a separate analysis.

In terms of new variables

$$\mathcal{P}(q) = \frac{\Delta_0^2}{1 + (gq_*/q) \ln |q/\beta gq_*|} \quad \mathcal{P}_T(q) = \frac{\Delta_{0T}^2}{1 + (g_t q_*/q) \ln |q/\beta_t g_t q_*|} \quad (15)$$

where

$$\Delta_0^2 = \frac{1}{4\pi^2 N^2 f_0}, \quad \Delta_{0T}^2 = \frac{2}{\pi^2 N^2 f_{T0}}. \quad (16)$$

We emphasize that these formulae were derived using perturbation theory, so our first task when fitting to data is to assess whether the perturbative expansion is justified at all scales seen by Planck. We use as an indication of the breakdown of perturbation theory the size of gq_*/q . Note that, unlike [40], we did not set $\beta = 1$. The theoretical computation [44] shows that generically $\beta \neq 1$, and furthermore, $\beta = 1$ provides a bad fit to the data (see Figure 6 or Table II). We are thus forced to use 3 parameters to fit the primordial spectrum, one more than needed for Λ CDM in (1).

Note that the form of the power spectrum (15) is a universal prediction for this class of theories, so if this form is disfavoured by the data then it rules out this class of holographic models. On the other hand, if (15) is consistent with data, one can further analyze whether the best fit values can be reproduced by a specific choice of QFT within this class.

C. Empirical models

To formalize the comparison we now define (following [40]) the empirical model of holographic cosmology (HC) to be the model parametrized by the seven parameters $(\Omega_b h^2, \Omega_c h^2, \theta, \tau, \Delta_0^2, g, \ln \beta)$, where $\Omega_b h^2$ and $\Omega_c h^2$ are the baryon and dark matter densities, θ is the angular size of the sound horizon at recombination and τ is the optical depth due to re-ionization.

This model is to be compared with Λ CDM, which is parametrized by six parameters, $(\Omega_b h^2, \Omega_c h^2, \theta, \tau, \Delta_0^2, n_s)$ and Δ_0^2, n_s are the parameters entering in (1).

We also compare HC with Λ CDM with running, which includes as a new parameter the running $\alpha_s = dn_s/d \ln q$. In this case the scalar power spectrum is given by

$$\mathcal{P}(q) = \Delta_0^2 \left(\frac{q}{q_*} \right)^{(n_s-1) + \frac{\alpha_s}{2} \ln \left(\frac{q}{q_*} \right)}. \quad (17)$$

The running is usually set to zero since it does not improve the fitting significantly. Here we include this model so that we can also compare HC to a model with the same number of parameters.

In inflationary models, n_s typically has weak dependence on q and it may be Taylor expanded around q_* . In Λ CDM, one keeps the leading order term in this expansion, while in Λ CDM with running one keeps in addition the sub-leading term. In slow-roll inflation, the running is second order in slow-roll parameters and higher order running is further suppressed [47]. The holographic power spectrum (15) can be rewritten in the form (1) with specific $n_s = n_s(q)$ when $gq_*/q \ll 1$. In this case, however, $\alpha_s/(n_s - 1) = -1$, and higher order runnings are not suppressed [11, 40].

All the cosmological parameters other than those quantifying the primordial spectrum – i.e. those in the transfer function – are the same in all three models. In addition, all three models have a parameter Δ_0^2 which determines the overall amplitude of the power

TABLE I. Priors for CosmoMC. The priors are the default for CosmoMC for the Λ CDM parameters. g and β ranges were chosen to ensure viability of the primordial power spectrum.

Parameter	Minimum	Maximum
$\Omega_b h^2$	0.005	0.1
$\Omega_c h^2$	0.001	0.99
100θ	0.5	10
τ	0.01	0.8
$\ln(10^{10}\Delta_0^2)$	2	4
n_s (Λ CDM)	0.8	1.2
α_s (Λ CDM running)	-0.05	0.05
g (HC)	-0.025	-0.001
$\ln\beta$ (HC)	-0.9	4

spectrum. These parameters are accounted for in the data analysis using CosmoMC by fitting for 100θ , τ , $\ln(10^{10}\Delta_0^2)$, $\Omega_b h^2$, and $\Omega_c h^2$. In addition, all the nuisance parameters of Planck are identical for both models. The values and details of these are considered irrelevant for the analysis. For the parameters not shared by the models, Λ CDM uses n_s and α_s if running is included. Holographic cosmology uses g and $\ln(\beta)$. The priors used for the relevant parameters are in Table I.

III. MATCHING THE MODEL TO DATA

A. Best Fit Parameters

In order to determine how well the models fit to data, we started by finding the best fit parameters, median and expected ranges using CosmoMC [48–54]. Because we needed to compare models with no variations besides the primordial power spectrum, we ran not only holographic cosmology (for which we needed to modify the code to use our primordial power spectrum), but also Λ CDM using the same dataset. We ran Λ CDM both with and without running. Running was used to ensure the likelihoods were compared between models with the same number of parameters, while fitting to Λ CDM without running was done since running has previously been found to not make a significant difference [55].

We fit the models to two different sets of datasets. For both cases, the datasets used were identical for holographic cosmology and both Λ CDM models. The first case is marked as the standard, full Planck run, or is not indicated as special. The data sets used in this case were Planck 2015 (low TEB+high l [HM] TT) as well as lensing [55–61], as well as Baryonic Acoustic Oscillations (BAO) [62–69] and BICEP2-Keck-Planck (BKP) polarization [70]. The second case, called the high- l run or the run without low l s, uses all the same data except does not use the portion of the Planck dataset corresponding to $l < 30$.

After running CosmoMC to get the distribution of parameters, we ran the minimizer [71] included with the code to find the best fit parameters as well as its likelihood.

This procedure leads to the parameter ranges in Table II for the best fit and 68% region of both models using the full Planck dataset. As can be seen, the difference in χ^2 is 4.81. This means the difference between the models is 2.2σ , favouring Λ CDM. The difference in

TABLE II. Planck 2015 and BAO best fit parameters and 68% ranges for holographic cosmology and Λ CDM. Data for Λ CDM is from a separate run of CosmoMC, included to compare the χ^2 numbers.

	HC		Λ CDM		Λ CDM with running	
	best fit	68% range	best fit	68% range	best fit	68% range
$\Omega_b h^2$	0.02217	0.02215 ± 0.00021	0.02227	0.02225 ± 0.00020	0.02231	0.02229 ± 0.00022
$\Omega_c h^2$	0.1173	0.1172 ± 0.0012	0.1185	0.1186 ± 0.0012	0.1184	0.1186 ± 0.0012
100θ	1.04112	1.04115 ± 0.00042	1.04103	1.04104 ± 0.00042	1.04108	1.04105 ± 0.00041
τ	0.081	0.082 ± 0.013	0.067	0.067 ± 0.013	0.069	0.068 ± 0.013
$10^9 \Delta_0^2$	2.126	2.126 ± 0.058	2.143	2.143 ± 0.052	2.151	2.149 ± 0.054
n_s			0.9682	0.9677 ± 0.0045	0.9682	0.9671 ± 0.0045
α_s					-0.0027	-0.0030 ± 0.0074
g	-0.0070	$-0.0074^{+0.0014}_{-0.0013}$				
$\ln \beta$	0.88	$0.87^{+0.19}_{-0.24}$				
χ^2	11324.5		11319.9		11319.6	

likelihood between Λ CDM with and without running is less than 1, so the case with fewer parameters should be favoured. Our fit for Λ CDM is comparable to those found by the Planck team.

As mentioned earlier, the perturbative expansion (15) requires $|(gq^*)/q| \ll 1$. How large of values of $|(gq^*)/q|$ one is willing to accept depends on the error one is willing to tolerate. Certainly values of $|(gq^*)/q|$ which are of order 1 are outside the regime of validity of perturbation theory. In our case, as can be seen in Table II, the best fit value is $g = -0.00703$ and one can check that $2 \times 10^{-3} \leq |(gq^*)/q| \leq 2.5$, for the multipoles $2500 \leq l \leq 2$ seen by Planck. Therefore, $|(gq^*)/q|$ is indeed very small for almost all multipoles, but it does become large at very low multipoles (at $l = 30$ it is equal to 0.15, at $l = 20$ it is 0.25 and at $l = 2$ it is 2.5). It follows that perturbation theory is valid at all scales seen in Planck, except at very low multipoles. This is our first major conclusion: the data *a posteriori* justify the perturbative treatment for all multipoles but the very low ones.

At very low multipoles one cannot trust the model: a non-perturbative computation of the 2-point function of the energy-momentum tensor is needed in order to work out the predictions of this model for these multipoles. In order to stay within the regime of validity of the model, we therefore removed the low l data from our dataset and recalculated the parameters. The exact boundary at $l = 30$ was determined by the datasets we had from Planck, which offers the data already split between the $l < 30$ and $l \geq 30$ data and it is roughly in accordance with the estimate above. In [41] we further determined which model within the class of (8) reproduces the best fit values and within that model one can make a more precise estimate of the point where the perturbative treatment is not justified and this leads to $l \sim 35$.

Consequently, the results of the new fits can be found in Table III if we exclude $l < 30$. For this case, the difference in χ^2 is less than 1, indicating that the models are within 1.0σ of each other and that neither model is favoured. This is our second major conclusion: within their regimes of validity HC and Λ CDM fit the data equally well.

Figure 2 shows the shape and degeneracies of the most likely region of parameter space. The most obvious aspect of these figures is the irregular shape of $\ln(\beta)$ for the case when the

TABLE III. Same as Table II, but with $l < 30$ data removed for both holographic cosmology and Λ CDM.

	HC		Λ CDM		Λ CDM with running	
	best fit	68% range	best fit	68% range	best fit	68% range
$\Omega_b h^2$	0.02204	0.02202 ± 0.00022	0.02227	0.02224 ± 0.00020	0.02217	0.02212 ± 0.00024
$\Omega_c h^2$	0.1187	0.1187 ± 0.0014	0.1187	0.1188 ± 0.0013	0.1186	0.1188 ± 0.0013
100θ	1.04097	1.04099 ± 0.00042	1.04108	1.04104 ± 0.00043	1.04101	1.04100 ± 0.00041
τ	0.067	0.066 ± 0.017	0.0703	0.068 ± 0.016	0.0695	0.067 ± 0.016
$10^9 \Delta_0^2$	2.044	2.043 ± 0.074	2.158	2.151 ± 0.064	2.151	2.139 ± 0.066
n_s			0.9667	0.9660 ± 0.0048	0.9682	0.9666 ± 0.0047
α_s					0.0083	0.0090 ± 0.0094
g	-0.0130	$-0.0127^{+0.0042}_{-0.0038}$				
$\ln \beta$	1.01	$0.90^{+0.32}_{-0.16}$				
χ^2	824.0		824.5		823.5	

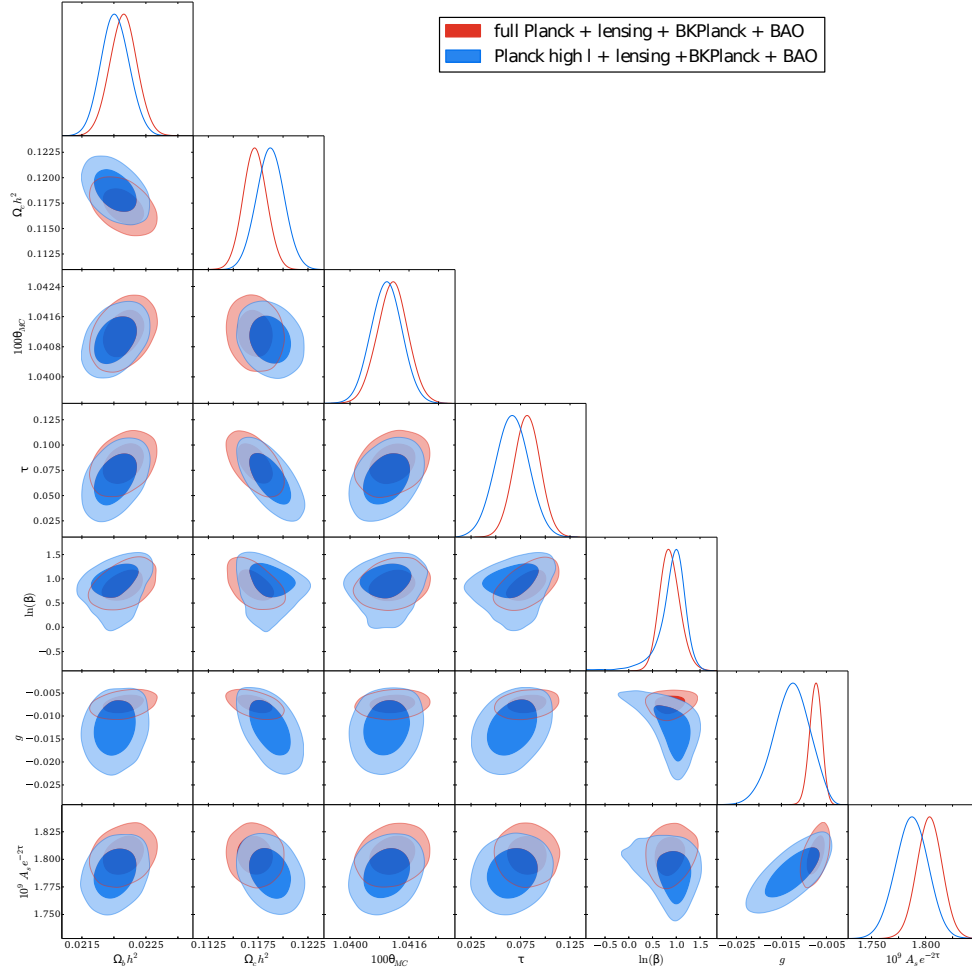


FIG. 2. A triangle plot of the likelihoods of parameters for holographic cosmology. The blue plots showing the case without low l s is less symmetric than the red plots with the full data set due to the reduced amount of data. The contours show the 68% and 95% confidence levels.

low l data is removed. This is seen somewhat in the 1σ region, but more clearly in the 2σ region. This seems to imply that $\ln(\beta)$ becomes less constrained and potentially consistent with 0 when the low l s are removed. The rest of the figure is comparable to Figure 43 of [57], although the degeneracy between Δ_0^2 and g is in the opposite direction of that between Δ_0^2 and n_s in that figure.

Taking the parameters from the case with the low- l data removed, we show the TT angular power spectra in Figure 3 for Planck 2015 data, as well as Λ CDM and holographic cosmology. Both models appear to fit the data equally well, with the difference between them being within the 68% region of Planck. Small l 's have the largest difference between the models, however the difference still remains within the error as low l s were not part of

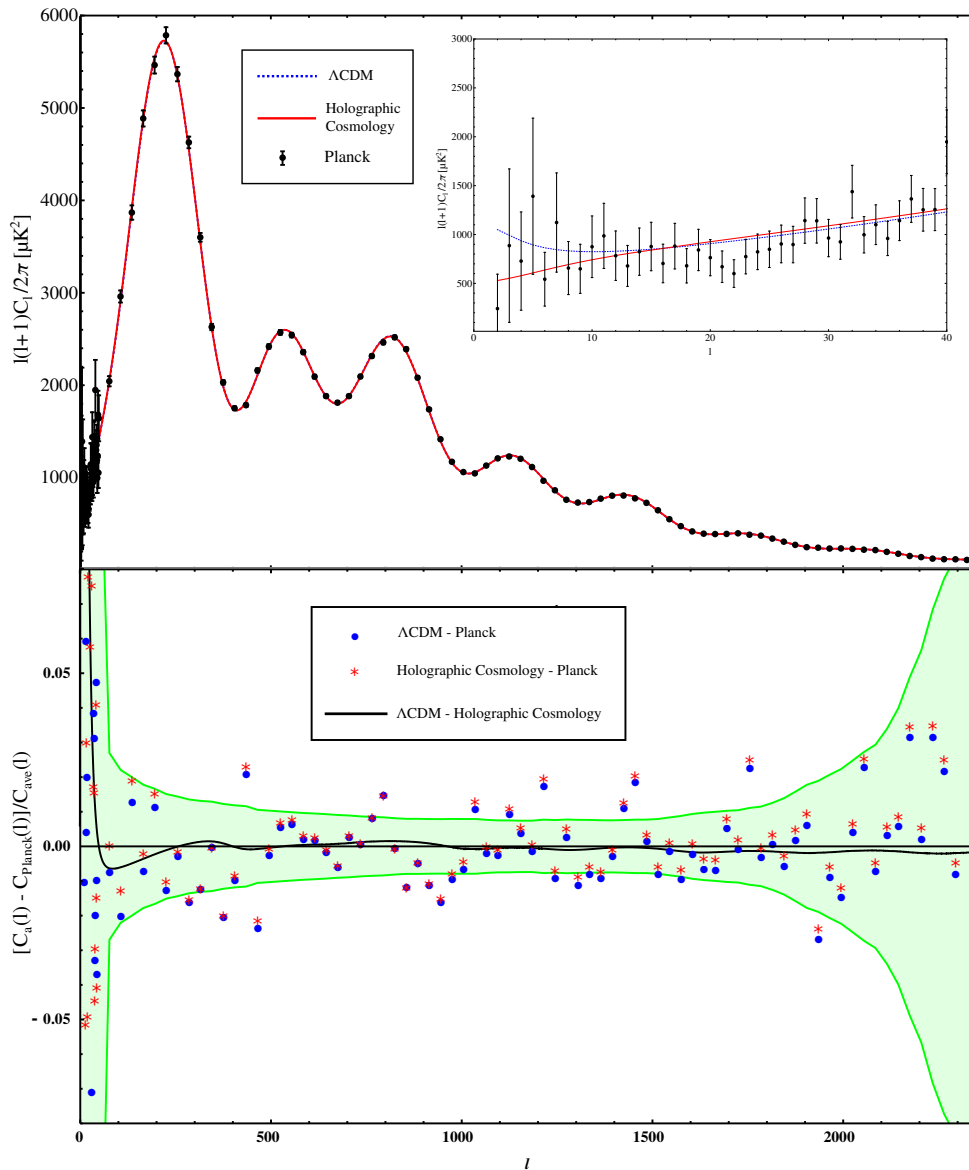


FIG. 3. TT power spectra of Planck 2015, Λ CDM and HC. Error bars are shown for low l . In the insert ($l \leq 40$), the blue line (Λ CDM) is noticeably above the red one (HC). The green shaded region in the difference plot shows the Planck relative error.

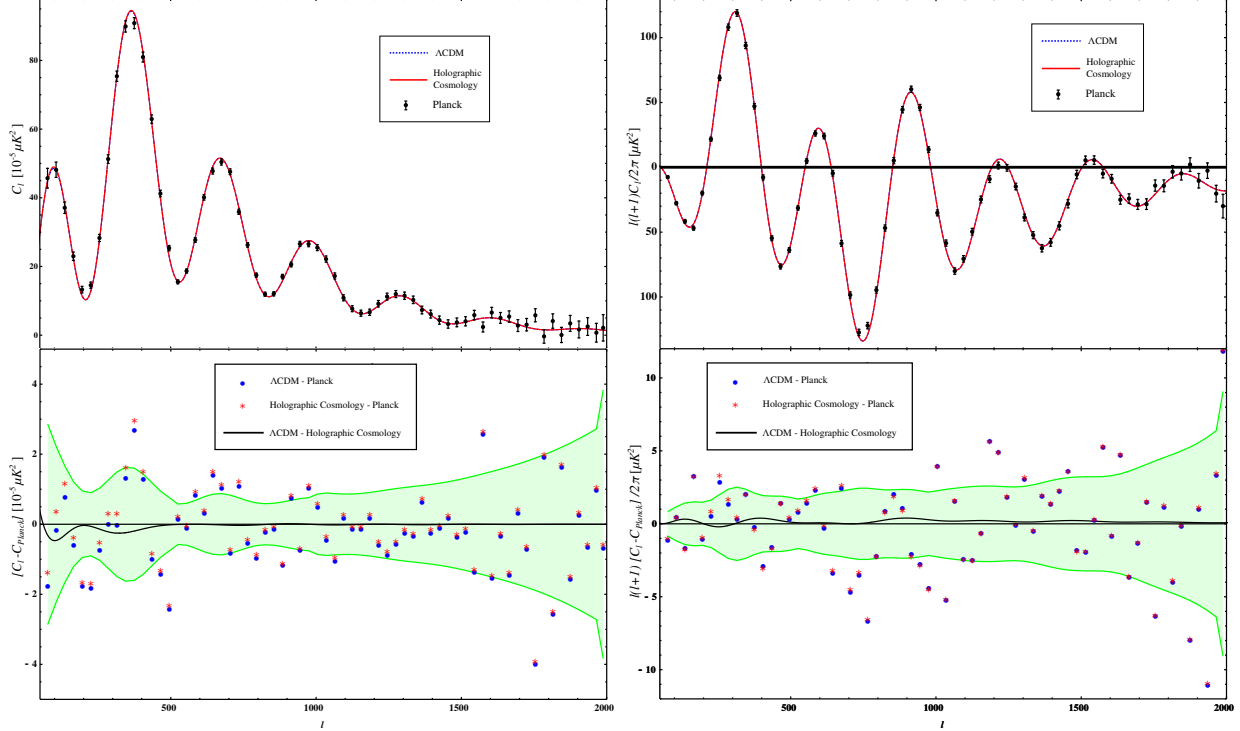


FIG. 4. Plots of EE (left) and TE (right) polarization for Planck 2015 (black), Λ CDM (blue) and HC (red). The green shaded region in the difference plot shows the Planck error.

calculating the fit.

Similar plots for the TE and EE power spectra are shown in Figure 4. These plots do not include the low- l data however. The goodness of fit is similar to the TT case. The units for the C_l 's match those used in [55].

B. Comparing Primordial Spectra

Now that we have the best fit parameters, we can examine the difference between the two primordial power spectra. This can be seen in Figure 5. We use the best fit parameters for holographic cosmology and Λ CDM without running found in Table III. This means we again used the values for when the low l data was removed. The same plot with the best fit values from Table II or from much of either tables' indicated range for parameters would look similar to what is seen. The error is approximated by assuming the same relative error as the Planck TT power spectrum, using $l \approx q \times 14$ Gpc.

The biggest difference between the two is seen at low l values. The cutoff used of $l = 30$ is around $q = 0.002$ Mpc $^{-1}$. This removes much of the very low values of the holographic cosmology primordial power spectrum, but still occurs (in the middle of the insert) before the holographic cosmology's spectrum has become larger than that of Λ CDM. Despite being very similar in value for $q \gtrsim 0.002$ Mpc $^{-1}$, the HC and Λ CDM power spectra can be seen to have different shapes.

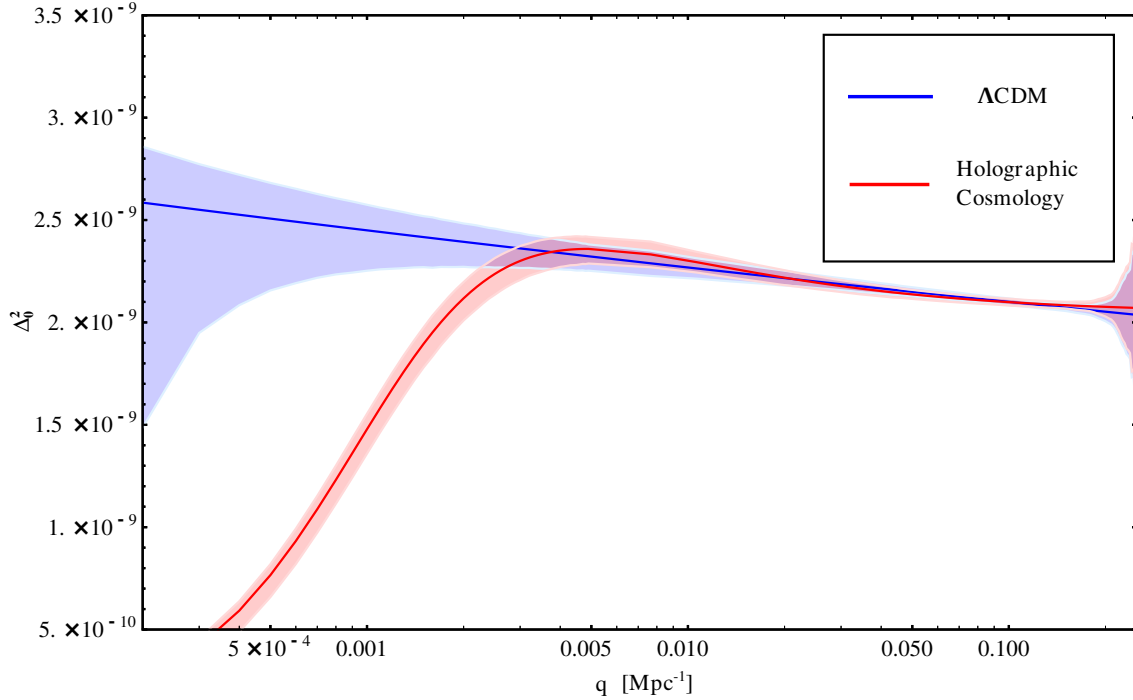


FIG. 5. Plot of the primordial power spectrum for HC and Λ CDM. The parameters used to produce the curves are the best fit values in Table III. The error (seen in the lighter shaded regions above and below the curves) is determined by assuming the same relative error as the Planck cl_s . It is included in order to give a sense of the error, not as the actual error. The red line indicating holographic cosmology starts significantly lower and increases rapidly at low q values.

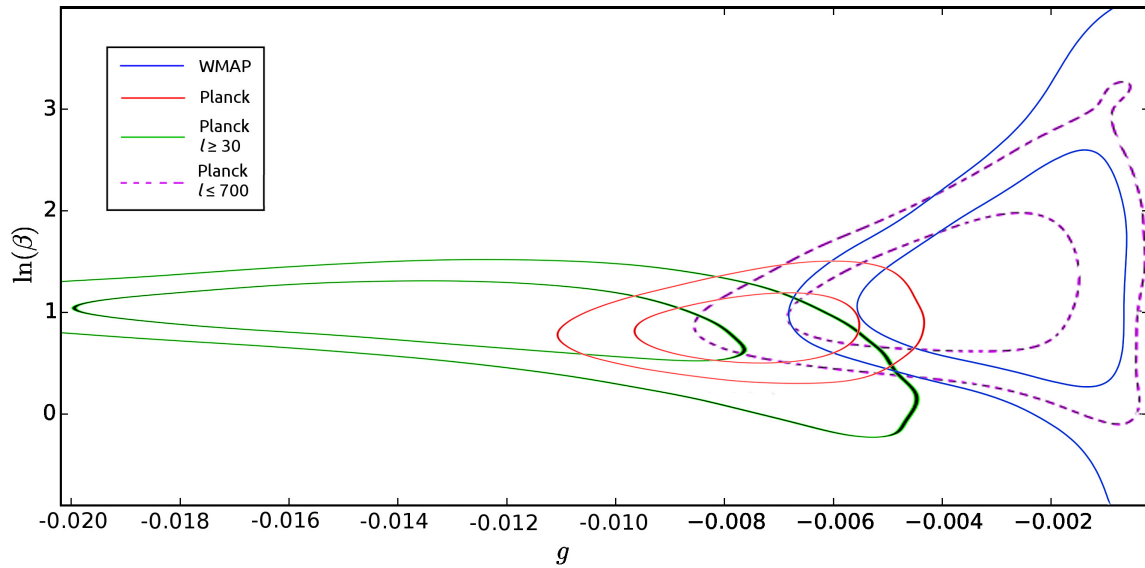


FIG. 6. Plot of 1σ and 2σ regions in parameter space for holographic cosmology g and $\ln(\beta)$ values for WMAP (blue, right), Planck (red, middle), Planck with low l values removed (green, left), and Planck with high l values removed (purple, dashed).

C. Comparison to Previous Results

Comparing the results for WMAP in [40] to the results for Planck here, it appears that g noticeably shifts to lower values, outside of the expected error. This shift remained when we reran the code for WMAP, this time including β and the same external datasets as we used for Planck.⁸ The trend towards more negative values of g continues when the low l dataset is removed from the data used to determine the parameters. This trend can be seen in Figure 6. While it is possible that this indicates an issue with the model, the theory, as stated previously, becomes non-perturbative when $|gq_*/q|$ becomes relatively large. This shift is believed to be compensating for the fact that the model is non-perturbative when using the full dataset. To test if the choice of range of l s is the reason for the shift in g , we also ran the Planck data without using any data for l above a chosen cutoff of $l = 700$ to mimic the uncertainty in the WMAP data for l s around that number.⁹ Despite the differences in the sharpness of the cutoff, the values found are close to those from WMAP.

A similar analysis for Λ CDM is shown in Figure 7. For this case, there is no similar shift in n_s and α_s . However, there is a known shift in τ from WMAP to Planck for the Λ CDM case: its best fit value went from 0.088 (WMAP) to 0.067 (Planck). Holographic cosmology with the full dataset gives $\tau = 0.081$ which goes down to 0.067 when we remove the $l < 30$ multipoles. The plot of n_s vs τ for Λ CDM is in Figure 8.

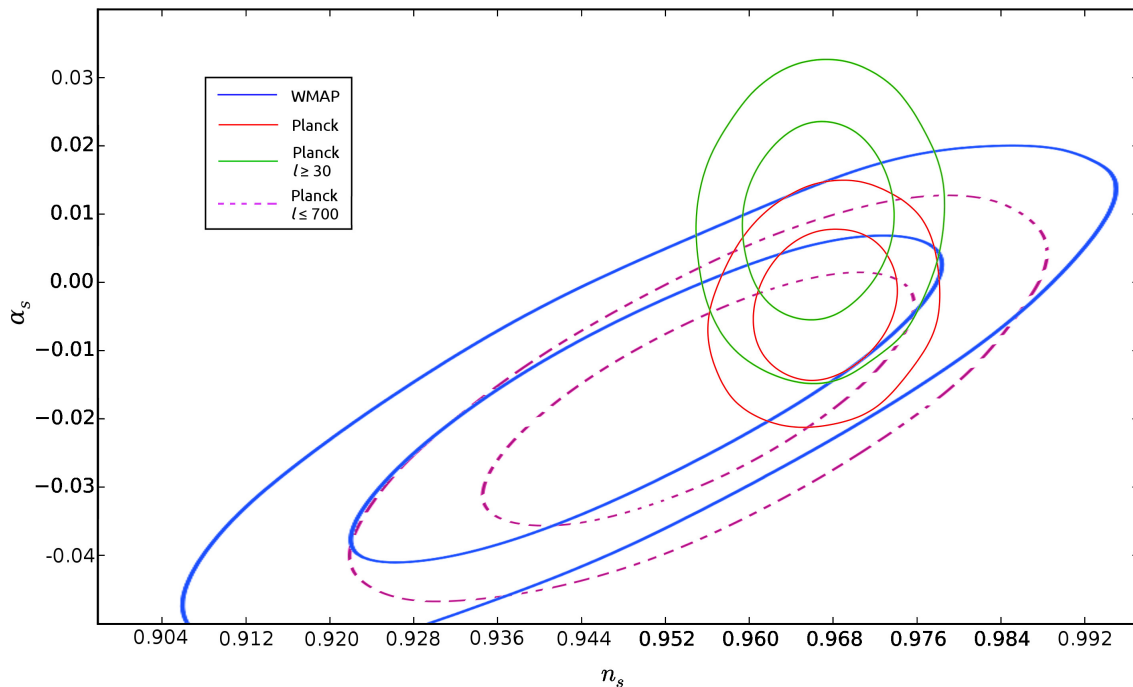


FIG. 7. Plot of 1σ and 2σ regions in parameter space of Λ CDM n_s and α_s values for WMAP (blue, largest pair of curves), Planck (red, below the green), Planck with low l values removed (green, above the red), and Planck with high l values removed (purple, dashed).

⁸ The parameter β was not used in [40] since it was (incorrectly) argued to be unimportant for the expected values of g . When we ran WMAP again using β (not setting it to 1), we got $\beta = 3.56$ and $g = -0.0027$. These values are used in Figure 6.

⁹ Because the data for $l > 30$ is binned every 30 l s, the cutoff point is not exactly $l = 700$. The code is then told to ignore the data for l s above the cutoff. The data still remains available to be used, however. This makes the cutoff imprecise. It is, however, sharper than WMAP, which has data for larger l s, but with a very large error. See [72] for discussions on this type of cutoff.

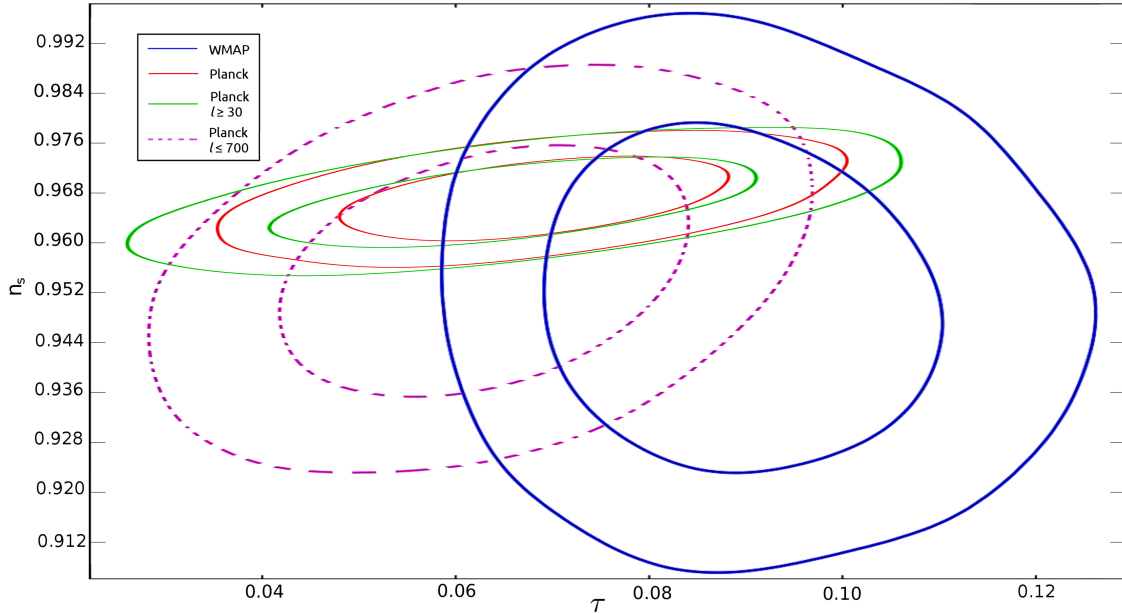


FIG. 8. Plot of 1σ and 2σ regions in the parameter space of Λ CDM n_s and τ values for WMAP (blue, largest pair of circles), Planck (red, the smallest set of circles), Planck with low l data removed (green, slightly larger than the red), and Planck with high l data removed (purple, dashed).

What we can see in these figures is that the shift in τ for Λ CDM appears due to Planck while the shift in g is at least partially due to the value of l . Since τ decreases to values similar to Planck when the low l data is removed (Table III), it appears that τ is decreased by Planck, but increased to fit the erroneous holographic cosmology power spectrum to compensate for the drop in the low l primordial power spectrum. We suspect that the lower τ value is real.

All other common parameters between the two models are compatible with each other.

D. Tensors

As in slow-roll inflation, holographic cosmology allows for the production of tensors. There are also holographic cosmology models consistent with an absence of tensors. The tensor affects which holographic models are possible, so an analysis of the status of tensors is required.

In holographic cosmology, the power spectrum for tensors is given in (15). The upper limit for the ratio of tensors to scalars, $r = \Delta_{0T}^2/\Delta_0^2$, is 12.49% for 2σ and 17.12% for 3σ . The data is consistent with $r = 0$. Figure 9 shows the triangle plot of these three parameters, showing that $r = 0$ is consistent with the data and consistent with any value of g_t or β_t . The allowed value of r can be increased, but this requires the values of $|g_t|$ and β_t to be increased past the point for which the perturbative expansion would be valid.

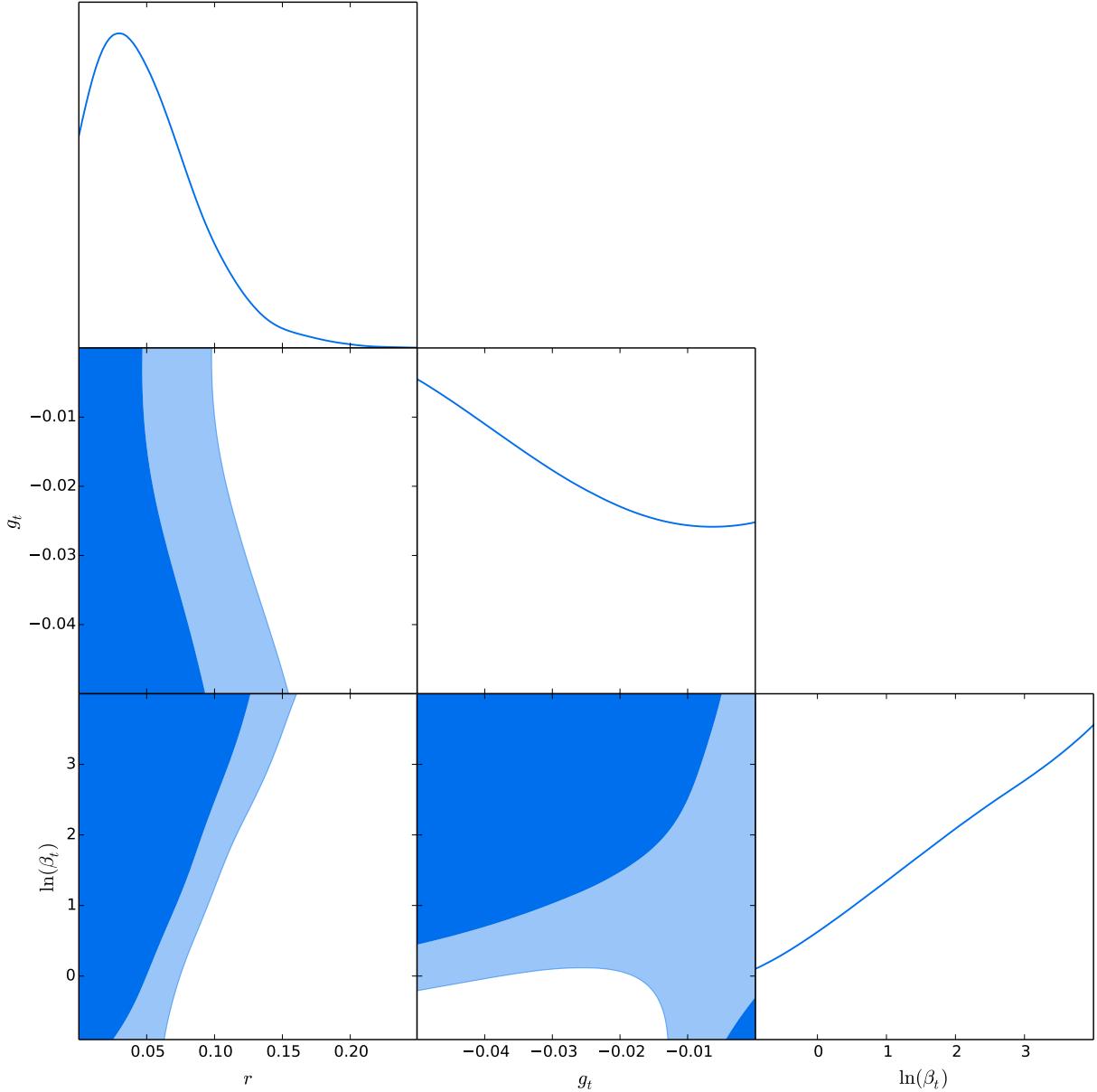


FIG. 9. A triangle plot of the likelihoods of parameters for tensors in holographic cosmology. The contours show the 68% and 95% confidence levels.

IV. MODEL EVIDENCE

In order to compare different models, one needs to determine which model is more likely given the data. Typically one determines which models fit the data better, using for instance the value of χ^2 or its square root. While this has already been noted (in Tables II and III), we examine these likelihoods further here. However, if what we want to know is the probability for the model given the data rather than the best fit of the model to the data we should use Bayesian Evidence. We emphasise that what we compare here are the empirical models introduced in Section II C.

TABLE IV. χ^2 breakdown for different runs of CosmoMC. The table shows the χ^2 values of the HC and Λ CDM with running from Table II (full Planck data) split by dataset. The χ^2 's are split into contributions from the high l dataset ($l \geq 30$), the low l dataset ($l < 30$) and all other contributions to χ^2 .

χ^2 breakdown for full Planck run (Table II)	HC	Λ CDM with running
Contribution of high l data ($l \geq 30$)	767.4	766.6
Contribution of low l data ($l < 30$)	10498.2	10494.1
Contribution of other data	58.9	58.9
Total contribution	11324.5	11319.6

TABLE V. χ^2 's, excluding $l < 30$ data, using best-fit parameters from Tables II and III.

	HC	Λ CDM with running
χ^2 for full Planck without low l data (from Table IV)	826.3	825.5
χ^2 total for $l \geq 30$ run (Table III)	824.0	823.5

A. Likelihoods

In order to compare the best fits of the two models, we calculate the difference in χ^2 . χ^2 is given by $\chi^2 = 2(-\ln \mathcal{L})$, where \mathcal{L} is the likelihood of the model. When we take the square root of the difference, $\sqrt{\Delta\chi^2}$, we can get the number of standard deviations one model is from the other. We interpret results within 1σ as insignificant, but a model is considered to be still viable at up to 3σ 's.

However, the likelihood does not account for the number of parameters in the model. Since we had to include β in the holographic cosmology models, we have one more parameter than standard Λ CDM. Instead of adding a term to compensate for the different number of parameters as suggested in [40], we added running to Λ CDM so that it has the same number of parameters. Increasing the number of parameters decreases the minimum χ^2 . Since this decrease, as seen in Table II, is less than 1, the extra parameter is disfavoured in the model. It does, however, give us a model with the same number of parameters for comparison.

The χ^2 values given in Tables II and III are also presented here in Table IV and V for holographic cosmology and Λ CDM with running. For the full Planck dataset, the difference in χ^2 is 4.81, corresponding to a difference of 2.2σ . However, as explained previously, our holographic model breaks down at low l values and cannot be trusted. Table IV shows the breakdown in the source of χ^2 based on dataset. As can be seen, most of this difference comes from low l data, which we do not expect to be accurate. Comparing instead the model run without the unreliable portions of the data, $\Delta\chi^2 = 0.5$. This is within 1σ , indicating that neither model is statistically preferred to the other.

B. Bayesian Evidence

In the previous subsection, we added a parameter (running) to Λ CDM in order to have models with the same number of parameters when we use likelihood to compare them. In this subsection, we use a method that automatically accounts for the number of parameters:

we compute the Bayesian evidence, the probability of each model given the data (rather than that of the data given the model). A detailed exposition of this method can be found in [73–75] and references therein. As reviewed in [40], application of Bayes’ theorem leads to

$$E = \int d\alpha_M P(\alpha_M) P(D|\alpha_M), \quad (18)$$

where α_M is the set of parameters that specify the model and D is the data. Here, $P(D|\alpha_M)$ is the probability for obtaining the data D given parameters α_M , which is the same as the likelihood $\mathcal{L}(\alpha_M)$ calculated previously. $P(\alpha_M)$ is the prior probability for the parameters.

Our aim is to compare the two empirical models introduced in Section II C and in order to be maximally agnostic about the underlying physical models we proceed by using flat priors, i.e. $P(\alpha_M) = \text{const.}$ for all values of α_M which we consider viable, while it vanishes otherwise. Then, the evidence integral becomes

$$E = \frac{1}{\text{Vol}_M} \int_{\text{Vol}_M} d\alpha_M \mathcal{L}(\alpha_M), \quad (19)$$

where the integral is over the region of the parameter space in which the prior probability distribution is non-zero and Vol_M is the volume of this region.

Alternatively, one could consider comparing physical models, for example a specific inflationary model versus the model specified by (8). In this case, the prior probabilities would (in principle) be theoretically computable from the underlying model. For the case of the holographic model in (8) the parameters g and β are related by a 2-loop computation to the parameters of the underlying model (the rank of the gauge group, the field content, the couplings etc.) and assuming that all perturbative models are *a priori* equally likely¹⁰ one can, in principle, compute the prior probability for the parameters g and β by analyzing how often given values of g and β are realized. It would be interesting to see whether such analysis would lead to non-trivial prior distribution. We leave such analysis to future work and proceed with flat priors, as is common.

To compute (19), we used MultiNest [76–78]. The priors are determined from the previous fits of the same empirical models to data and are given in Table VI. These priors were chosen to be consistent with the choices in [40]. However, the range of 100θ needed to be increased to allow for the known best fit values. In addition, the range of g_{min} needed to be increased to match the lower values of g . The range of g was chosen to be $g_{min} < g < 0$, with g_{min} variable. The upper limit was set to 0 as g was found to be negative in [40] (and the theoretical computation [41, 44] also shows that g is generically negative). The maximum $|g_{min}|$ reflects our expectation about the validity of the perturbative expansion. We allow for the possibility that the perturbative expansion is valid only for $l > 30$. We use as a rough estimate for the validity of perturbation theory that gq^*/q is sufficiently small, taking this to mean a value between 0.20 and 1 at $l = 30$.¹¹ This translates into $-0.009 < g_{min} < -0.45$. The prior for β is fixed by using the results from (our fit to) WMAP data. We use two sets of priors: one coming from the 1σ range ($0 \leq \ln \beta \leq 2$) and the other from the 2σ range ($-0.2 \leq \ln \beta \leq 3.5$). The prior for the running was taken to be $|\alpha_s| \leq 0.05$. This contains the 1σ region of α_s for all 1σ values of n_s for WMAP. It also contains up to the 2σ region for

¹⁰ Alternatively, one may use the partition function of the QFT (with no sources turned on) in order to assign different probabilities to different perturbative models.

¹¹ The momenta and multipoles are related via $q = l/r_h$, where $r_h = 14.2$ Gpc is the comoving radius of the last scattering surface.

TABLE VI. Priors used with MultiNest. g_{min} is variable and ranges from -0.009 to -0.65 . The priors are identical to those used for WMAP [40] except for 100θ and g which needed to be expanded to accommodate the best fit results and β and α_s which were not used originally.

Parameter	Minimum	Maximum
$\Omega_b h^2$	0.02	0.025
$\Omega_c h^2$	0.09	1.25
100θ	1.03	1.05
τ	0.02	1.5
$\ln(10^{10} * \Delta_0^2)$	2.9	3.3
n_s (Λ CDM, asymmetric)	0.92	1.0
n_s (Λ CDM, symmetric)	0.9	1.1
α_s (Λ CDM running)	-0.05	0.05
g (HC)	g_{min}	0
$\ln \beta$ (HC, small)	0	2
$\ln \beta$ (HC, large)	-0.2	3.5

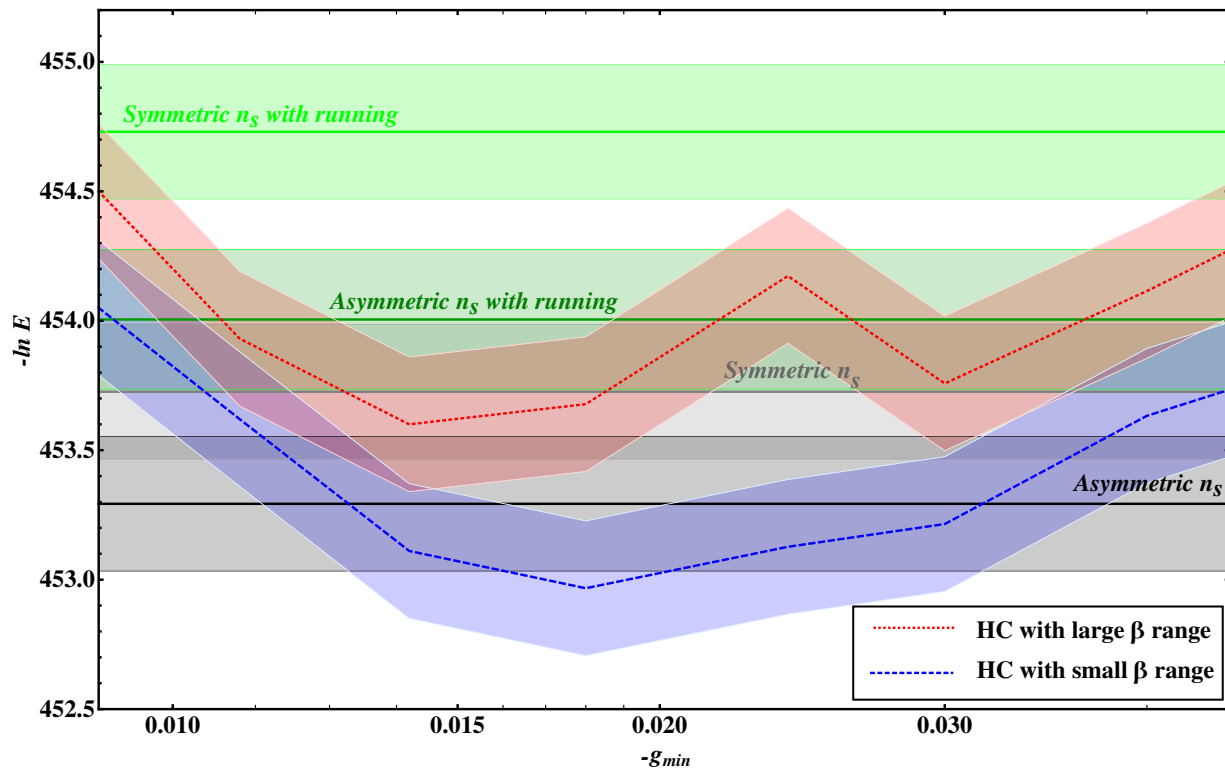


FIG. 10. Plot of Bayesian evidence when $l < 30$ data is removed. Priors are given in Table VI.

α_s independent of other parameters. Both this and the case with no running were calculated for Λ CDM.

In Figure 10, we present the results for the Bayesian evidence using the data without the low multipole and for different choices of priors. We use the data without the $l < 30$ multipoles because only for this portion of the data the holographic model is perturbative.

The shading around each line indicates the error. As a guide [74], a difference $\ln E < 1$ is insignificant and $2.5 < \ln E < 5$ is strongly significant. We can see that the difference in evidence between Λ CDM and holographic cosmology is insignificant.

V. CONCLUSION AND OUTLOOK

In this paper, we confronted holographic cosmology against Planck CMB anisotropy data, as well as other cosmological observations. In this work, holographic cosmology is the empirical model obtained by replacing the primordial power-law power spectrum assumed in Λ CDM by that obtained (holographically) by a perturbative computation in a three-dimensional superrenormalizable QFT with generalized conformal structure. We found that the data *a posteriori* justifies the use of perturbation theory for all but the very low-multipoles ($l < 30$). Restricting to this part of the data, we further found that this theory fits just as well as Λ CDM. This follows both from the goodness of fit (the difference of χ^2 is less than 1) and Bayesian evidence (the difference in log Bayesian evidence is less than one). If we (incorrectly) use the holographic model over the entire data, then the model is viable but disfavoured.

In order to include in the analysis the low-multipole data one would need a non-perturbative evaluation of the 2-point function of the energy momentum tensor. One way to do this is to put the QFT on lattice and use the methods of lattice gauge theory; such computation is currently in progress. Such non-perturbative results would allow us to meaningfully compare this model with Λ CDM over the entire data, and may potentially explain the large angle anomalies in the CMB sky (e.g., [79]). A lattice computation would also allow us to formulate yet another new class of the holographic models, namely ones based on a QFT with a coupling constant of intermediate strength. Such models could potentially provide an even better fit than the models we analysed.

In the analysis in this paper we assumed an instant reheating: the data from the end of the very early universe phase were the initial conditions for hot big bang cosmology. It would be useful to develop a dynamical model describing the transition from the non-geometric phase to Einstein gravity. This may be achieved by adding irrelevant operators that would modify the UV sector of the QFT and induce an RG flow that would drive the theory to strong coupling. Such terms could modify the high l part of the spectrum, but our ability to fit the current data very well without such corrections suggests that they are small. However, future results from the next generation stage IV CMB experiments [80], as well as future large scale structure surveys such as SPHEREX [81], are expected to reach up to much higher wavenumbers, potentially probing the holographic reheating phase in our model.

ACKNOWLEDGMENTS

We would like to thank Raphael Flauger for collaboration at early stages of this work. KS is supported in part by the Science and Technology Facilities Council (Consolidated Grant “Exploring the Limits of the Standard Model and Beyond”). NA and EG were supported in part by the University of Waterloo, Natural Sciences and Engineering Research Council of Canada (NSERC), and Perimeter Institute for Theoretical Physics. Research at Perimeter Institute is supported by the Government of Canada through the Department

of Innovation, Science and Economic Development Canada and by the Province of Ontario through the Ministry of Research, Innovation and Science. This project has received funding from the European Union’s Horizon 2020 research and innovation programme under the Marie Skłodowska-Curie grant agreement No 690575. We acknowledge the use of the Legacy Archive for Microwave Background Data Analysis (LAMBDA), part of the High Energy Astrophysics Science Archive Center (HEASARC). HEASARC/LAMBDA is a service of the Astrophysics Science Division at the NASA Goddard Space Flight Center.

-
- [1] Robert H. Brandenberger, “Inflationary Cosmology: Progress and Problems,” arXiv:hep-ph/9910410 [hep-ph].
 - [2] Gerard ’t Hooft, “Dimensional reduction in quantum gravity,” in *Salamfest 1993:0284-296* (1993) pp. 0284–296, arXiv:gr-qc/9310026 [gr-qc].
 - [3] Leonard Susskind, “The World as a hologram,” *J. Math. Phys.* **36**, 6377–6396 (1995), arXiv:hep-th/9409089 [hep-th].
 - [4] Juan Martin Maldacena, “The Large N limit of superconformal field theories and supergravity,” *Int. J. Theor. Phys.* **38**, 1113–1133 (1999), [Adv. Theor. Math. Phys.2,231(1998)], arXiv:hep-th/9711200 [hep-th].
 - [5] C. M. Hull, “Timelike T duality, de Sitter space, large N gauge theories and topological field theory,” *JHEP* **07**, 021 (1998), arXiv:hep-th/9806146 [hep-th].
 - [6] Edward Witten, “Quantum gravity in de Sitter space,” in *Strings 2001: International Conference Mumbai, India, January 5-10, 2001* (2001) arXiv:hep-th/0106109 [hep-th].
 - [7] Andrew Strominger, “The dS / CFT correspondence,” *JHEP* **10**, 034 (2001), arXiv:hep-th/0106113 [hep-th].
 - [8] Andrew Strominger, “Inflation and the dS / CFT correspondence,” *JHEP* **11**, 049 (2001), arXiv:hep-th/0110087 [hep-th].
 - [9] Juan Martin Maldacena, “Non-Gaussian features of primordial fluctuations in single field inflationary models,” *JHEP* **05**, 013 (2003), arXiv:astro-ph/0210603 [astro-ph].
 - [10] Paul McFadden and Kostas Skenderis, “Holography for Cosmology,” *Phys. Rev.* **D81**, 021301 (2010), arXiv:0907.5542 [hep-th].
 - [11] Paul McFadden and Kostas Skenderis, “The Holographic Universe,” *Classical and quantum gravity. Proceedings, 1st Mediterranean Conference, MCCQG 2009, Kolymbari, Crete, Greece, September 14-18, 2009*, *J. Phys. Conf. Ser.* **222**, 012007 (2010), arXiv:1001.2007 [hep-th].
 - [12] Paul McFadden and Kostas Skenderis, “Holographic Non-Gaussianity,” *JCAP* **1105**, 013 (2011), arXiv:1011.0452 [hep-th].
 - [13] Paul McFadden and Kostas Skenderis, “Cosmological 3-point correlators from holography,” *JCAP* **1106**, 030 (2011), arXiv:1104.3894 [hep-th].
 - [14] Adam Bzowski, Paul McFadden, and Kostas Skenderis, “Holographic predictions for cosmological 3-point functions,” *JHEP* **03**, 091 (2012), arXiv:1112.1967 [hep-th].
 - [15] Kostas Skenderis and Paul K. Townsend, “Hidden supersymmetry of domain walls and cosmologies,” *Phys. Rev. Lett.* **96**, 191301 (2006), arXiv:hep-th/0602260 [hep-th].
 - [16] Juan M. Maldacena and Guilherme L. Pimentel, “On graviton non-Gaussianities during inflation,” *JHEP* **09**, 045 (2011), arXiv:1104.2846 [hep-th].
 - [17] James B. Hartle, S. W. Hawking, and Thomas Hertog, “Accelerated Expansion from Negative Λ ,” (2012), arXiv:1205.3807 [hep-th].

- [18] James B. Hartle, S. W. Hawking, and Thomas Hertog, “Quantum Probabilities for Inflation from Holography,” *JCAP* **1401**, 015 (2014), arXiv:1207.6653 [hep-th].
- [19] Koenraad Schalm, Gary Shiu, and Ted van der Aalst, “Consistency condition for inflation from (broken) conformal symmetry,” *JCAP* **1303**, 005 (2013), arXiv:1211.2157 [hep-th].
- [20] Adam Bzowski, Paul McFadden, and Kostas Skenderis, “Holography for inflation using conformal perturbation theory,” *JHEP* **04**, 047 (2013), arXiv:1211.4550 [hep-th].
- [21] Ishan Mata, Suvrat Raju, and Sandip Trivedi, “CMB from CFT,” *JHEP* **07**, 015 (2013), arXiv:1211.5482 [hep-th].
- [22] Jaume Garriga and Yuko Urakawa, “Inflation and deformation of conformal field theory,” *JCAP* **1307**, 033 (2013), arXiv:1303.5997 [hep-th].
- [23] Paul McFadden, “On the power spectrum of inflationary cosmologies dual to a deformed CFT,” *JHEP* **10**, 071 (2013), arXiv:1308.0331 [hep-th].
- [24] Archisman Ghosh, Nilay Kundu, Suvrat Raju, and Sandip P. Trivedi, “Conformal Invariance and the Four Point Scalar Correlator in Slow-Roll Inflation,” *JHEP* **07**, 011 (2014), arXiv:1401.1426 [hep-th].
- [25] Jaume Garriga and Yuko Urakawa, “Holographic inflation and the conservation of ζ ,” *JHEP* **06**, 086 (2014), arXiv:1403.5497 [hep-th].
- [26] Nilay Kundu, Ashish Shukla, and Sandip P. Trivedi, “Constraints from Conformal Symmetry on the Three Point Scalar Correlator in Inflation,” *JHEP* **04**, 061 (2015), arXiv:1410.2606 [hep-th].
- [27] Jaume Garriga, Kostas Skenderis, and Yuko Urakawa, “Multi-field inflation from holography,” *JCAP* **1501**, 028 (2015), arXiv:1410.3290 [hep-th].
- [28] Paul McFadden, “Soft limits in holographic cosmology,” *JHEP* **02**, 053 (2015), arXiv:1412.1874 [hep-th].
- [29] Nima Arkani-Hamed and Juan Maldacena, “Cosmological Collider Physics,” (2015), arXiv:1503.08043 [hep-th].
- [30] Nilay Kundu, Ashish Shukla, and Sandip P. Trivedi, “Ward Identities for Scale and Special Conformal Transformations in Inflation,” *JHEP* **01**, 046 (2016), arXiv:1507.06017 [hep-th].
- [31] Thomas Hertog and Ellen van der Woerd, “Primordial fluctuations from complex AdS saddle points,” *JCAP* **1602**, 010 (2016), arXiv:1509.03291 [hep-th].
- [32] Jaume Garriga, Yuko Urakawa, and Filippo Vernizzi, “ δN formalism from superpotential and holography,” *JCAP* **1602**, 036 (2016), arXiv:1509.07339 [hep-th].
- [33] Jaume Garriga and Yuko Urakawa, “Consistency relations and conservation of ζ in holographic inflation,” (2016), arXiv:1606.04767 [hep-th].
- [34] Nissan Itzhaki, Juan Martin Maldacena, Jacob Sonnenschein, and Shimon Yankielowicz, “Supergravity and the large N limit of theories with sixteen supercharges,” *Phys. Rev.* **D58**, 046004 (1998), arXiv:hep-th/9802042 [hep-th].
- [35] H. J. Boonstra, K. Skenderis, and P. K. Townsend, “The domain wall / QFT correspondence,” *JHEP* **01**, 003 (1999), arXiv:hep-th/9807137 [hep-th].
- [36] Ingmar Kanitscheider, Kostas Skenderis, and Marika Taylor, “Precision holography for non-conformal branes,” *JHEP* **09**, 094 (2008), arXiv:0807.3324 [hep-th].
- [37] Claudio Corianò, Luigi Delle Rose, and Mirko Serino, “Three and Four Point Functions of Stress Energy Tensors in D=3 for the Analysis of Cosmological Non-Gaussianities,” *JHEP* **12**, 090 (2012), arXiv:1210.0136 [hep-th].
- [38] Shinsuke Kawai and Yu Nakayama, “Improvement of energy-momentum tensor and non-Gaussianities in holographic cosmology,” *JHEP* **06**, 052 (2014), arXiv:1403.6220 [hep-th].

- [39] Mafalda Dias, “Cosmology at the boundary of de Sitter using the dS/QFT correspondence,” *Phys. Rev.* **D84**, 023512 (2011), arXiv:1104.0625 [astro-ph.CO].
- [40] Richard Easther, Raphael Flauger, Paul McFadden, and Kostas Skenderis, “Constraining holographic inflation with WMAP,” *JCAP* **1109**, 030 (2011), arXiv:1104.2040 [astro-ph.CO].
- [41] Niayesh Afshordi, Claudio Coriano, Luigi Delle Rose, Elizabeth Gould, and Kostas Skenderis, “From Planck data to Planck era: Observational tests of Holographic Cosmology,” *Phys. Rev. Lett.* **118**, 041301 (2017), arXiv:1607.04878 [astro-ph.CO].
- [42] Dionysios Anninos, Thomas Hartman, and Andrew Strominger, “Higher Spin Realization of the dS/CFT Correspondence,” *Class. Quant. Grav.* **34**, 015009 (2017), arXiv:1108.5735 [hep-th].
- [43] Antal Jevicki, Yoichi Kazama, and Tamiaki Yoneya, “Generalized conformal symmetry in D-brane matrix models,” *Phys. Rev.* **D59**, 066001 (1999), arXiv:hep-th/9810146 [hep-th].
- [44] Claudio Corianò, Luigi Delle Rose, and Kostas Skenderis, “Quantum Field Theory with generalized conformal structure,” (2017), to appear.
- [45] R. Jackiw and S. Templeton, “How Superrenormalizable Interactions Cure their Infrared Divergences,” *Phys. Rev.* **D23**, 2291 (1981).
- [46] Thomas Appelquist and Robert D. Pisarski, “High-Temperature Yang-Mills Theories and Three-Dimensional Quantum Chromodynamics,” *Phys. Rev.* **D23**, 2305 (1981).
- [47] Arthur Kosowsky and Michael S. Turner, “CBR anisotropy and the running of the scalar spectral index,” *Phys. Rev.* **D52**, 1739–1743 (1995), arXiv:astro-ph/9504071 [astro-ph].
- [48] Uros Seljak and Matias Zaldarriaga, “A line of sight approach to cosmic microwave background anisotropies,” *Astrophys. J.* **469**, 437–444 (1996), astro-ph/9603033.
- [49] Matias Zaldarriaga, Uros Seljak, and Edmund Bertschinger, “Integral solution for the microwave background anisotropies in nonflat universes,” *Astrophys. J.* **494**, 491–502 (1998), arXiv:astro-ph/9704265 [astro-ph].
- [50] Antony Lewis, Anthony Challinor, and Anthony Lasenby, “Efficient computation of CMB anisotropies in closed FRW models,” *Astrophys. J.* **538**, 473–476 (2000), arXiv:astro-ph/9911177 [astro-ph].
- [51] Antony Lewis and Sarah Bridle, “Cosmological parameters from CMB and other data: A Monte Carlo approach,” *Phys. Rev.* **D66**, 103511 (2002), arXiv:astro-ph/0205436 [astro-ph].
- [52] Cullan Howlett, Antony Lewis, Alex Hall, and Anthony Challinor, “CMB power spectrum parameter degeneracies in the era of precision cosmology,” *JCAP* **1204**, 027 (2012), arXiv:1201.3654 [astro-ph.CO].
- [53] Antony Lewis, “Efficient sampling of fast and slow cosmological parameters,” *Phys. Rev.* **D87**, 103529 (2013), arXiv:1304.4473 [astro-ph.CO].
- [54] Antony Lewis, “CAMB Notes,” <http://cosmologist.info/notes/CAMB.pdf>.
- [55] P. A. R. Ade *et al.* (Planck), “Planck 2015 results. XIII. Cosmological parameters,” (2015), arXiv:1502.01589 [astro-ph.CO].
- [56] P.A.R. Ade *et al.* (Planck), “Planck 2015 results. XV. Gravitational lensing,” (2015), arXiv:1502.01591 [astro-ph.CO].
- [57] N. Aghanim *et al.* (Planck), “Planck 2015 results. XI. CMB power spectra, likelihoods, and robustness of parameters,” (2015), arXiv:1507.02704 [astro-ph.CO].
- [58] P.A.R. Ade *et al.* (Planck), “Planck 2015 results. XXIV. Cosmology from Sunyaev-Zeldovich cluster counts,” (2015), arXiv:1502.01597 [astro-ph.CO].
- [59] C.L. Bennett *et al.* (WMAP), “Nine-Year Wilkinson Microwave Anisotropy Probe (WMAP) Observations: Final Maps and Results,” *Astrophys. J. Suppl.* **208**, 20 (2013), arXiv:1212.5225

- [astro-ph.CO].
- [60] C.L. Reichardt, L. Shaw, O. Zahn, K.A. Aird, B.A. Benson, *et al.*, “A measurement of secondary cosmic microwave background anisotropies with two years of South Pole Telescope observations,” *Astrophys.J.* **755**, 70 (2012), arXiv:1111.0932 [astro-ph.CO].
- [61] Sudeep Das, Thibaut Louis, Michael R. Nolta, Graeme E. Addison, Elia S. Battistelli, *et al.*, “The Atacama Cosmology Telescope: temperature and gravitational lensing power spectrum measurements from three seasons of data,” *JCAP* **1404**, 014 (2014), arXiv:1301.1037 [astro-ph.CO].
- [62] Florian Beutler, Chris Blake, Matthew Colless, D. Heath Jones, Lister Staveley-Smith, *et al.*, “The 6dF Galaxy Survey: Baryon Acoustic Oscillations and the Local Hubble Constant,” *Mon.Not.Roy.Astron.Soc.* **416**, 3017–3032 (2011), arXiv:1106.3366 [astro-ph.CO].
- [63] Chris Blake, Eyal Kazin, Florian Beutler, Tamara Davis, David Parkinson, *et al.*, “The WiggleZ Dark Energy Survey: mapping the distance-redshift relation with baryon acoustic oscillations,” *Mon.Not.Roy.Astron.Soc.* **418**, 1707–1724 (2011), arXiv:1108.2635 [astro-ph.CO].
- [64] Lauren Anderson *et al.*, “The clustering of galaxies in the SDSS-III Baryon Oscillation Spectroscopic Survey: Baryon Acoustic Oscillations in the Data Release 9 Spectroscopic Galaxy Sample,” *Mon. Not. Roy. Astron. Soc.* **427**, 3435–3467 (2013), arXiv:1203.6594 [astro-ph.CO].
- [65] Florian Beutler, Chris Blake, Matthew Colless, D. Heath Jones, Lister Staveley-Smith, *et al.*, “The 6dF Galaxy Survey: $z \approx 0$ measurement of the growth rate and σ_8 ,” *Mon.Not.Roy.Astron.Soc.* **423**, 3430–3444 (2012), arXiv:1204.4725 [astro-ph.CO].
- [66] Nikhil Padmanabhan, Xiaoying Xu, Daniel J. Eisenstein, Richard Scalzo, Antonio J. Cuesta, Kushal T. Mehta, and Eyal Kazin, “A 2 per cent distance to $z=0.35$ by reconstructing baryon acoustic oscillations - I. Methods and application to the Sloan Digital Sky Survey,” *Mon. Not. Roy. Astron. Soc.* **427**, 2132–2145 (2012), arXiv:1202.0090 [astro-ph.CO].
- [67] Lauren Anderson *et al.* (BOSS), “The clustering of galaxies in the SDSS-III Baryon Oscillation Spectroscopic Survey: baryon acoustic oscillations in the Data Releases 10 and 11 Galaxy samples,” *Mon. Not. Roy. Astron. Soc.* **441**, 24–62 (2014), arXiv:1312.4877 [astro-ph.CO].
- [68] Lado Samushia, Beth A. Reid, Martin White, Will J. Percival, Antonio J. Cuesta, *et al.*, “The Clustering of Galaxies in the SDSS-III Baryon Oscillation Spectroscopic Survey (BOSS): measuring growth rate and geometry with anisotropic clustering,” *Mon.Not.Roy.Astron.Soc.* **439**, 3504–3519 (2014), arXiv:1312.4899 [astro-ph.CO].
- [69] Ashley J. Ross, Lado Samushia, Cullan Howlett, Will J. Percival, Angela Burden, and Marc Manera, “The clustering of the SDSS DR7 main Galaxy sample - I. A 4 per cent distance measure at $z = 0.15$,” *Mon. Not. Roy. Astron. Soc.* **449**, 835–847 (2015), arXiv:1409.3242 [astro-ph.CO].
- [70] P.A.R. Ade *et al.* (BICEP2, Planck), “Joint Analysis of BICEP2/*KeckArray* and *Planck* Data,” *Phys.Rev.Lett.* **114**, 101301 (2015), arXiv:1502.00612 [astro-ph.CO].
- [71] M.J.D. Powell, “The BOBYQA algorithm for bound constrained optimization without derivatives,” http://www.damtp.cam.ac.uk/user/na/NA_papers/NA2009_06.pdf.
- [72] N. Aghanim *et al.* (Planck), “Planck 2016 intermediate results. LI. Features in the cosmic microwave background temperature power spectrum and shifts in cosmological parameters,” (2016), arXiv:1608.02487 [astro-ph.CO].
- [73] E Jaynes, “Probability Theory: The Logic of Science,” Cambridge University Press (2003).
- [74] Roberto Trotta, “Bayes in the sky: Bayesian inference and model selection in cosmology,” *Contemp. Phys.* **49**, 71–104 (2008), arXiv:0803.4089 [astro-ph].
- [75] M. Hobson, A. Jaffe, A. Liddle, P. Mukherjee and D. Parkinson,, “Bayesian methods in cos-

- mology,” Cambridge University Press (2010).
- [76] Farhan Feroz and M. P. Hobson, “Multimodal nested sampling: an efficient and robust alternative to MCMC methods for astronomical data analysis,” *Mon. Not. Roy. Astron. Soc.* **384**, 449 (2008), arXiv:0704.3704 [astro-ph].
 - [77] F. Feroz, M. P. Hobson, and M. Bridges, “MultiNest: an efficient and robust Bayesian inference tool for cosmology and particle physics,” *Mon. Not. Roy. Astron. Soc.* **398**, 1601–1614 (2009), arXiv:0809.3437 [astro-ph].
 - [78] F. Feroz, M. P. Hobson, E. Cameron, and A. N. Pettitt, “Importance Nested Sampling and the MultiNest Algorithm,” (2013), arXiv:1306.2144 [astro-ph.IM].
 - [79] P. A. R. Ade *et al.* (Planck), “Planck 2013 results. XXIII. Isotropy and statistics of the CMB,” *Astron. Astrophys.* **571**, A23 (2014), arXiv:1303.5083 [astro-ph.CO].
 - [80] Kevork N. Abazajian *et al.* (CMB-S4), “CMB-S4 Science Book, First Edition,” (2016), arXiv:1610.02743 [astro-ph.CO].
 - [81] Olivier Dore *et al.*, “Cosmology with the SPHEREX All-Sky Spectral Survey,” (2014), arXiv:1412.4872 [astro-ph.CO].